Energy transfer networks: Quasicontinuum photoluminescence linked to high densities of defects

Ted A. Laurence,* Sonny Ly, Jeff D. Bude, Salmaan H. Baxamusa, Xavier Lepró, and Paul Ehrmann
Materials Science Division, Lawrence Livermore National Laboratory, Livermore, California 94550, USA
(Received 16 June 2017; published 6 November 2017)

In a series of studies related to laser-induced damage of optical materials and deposition of plastics, we discovered a broadly emitting photoluminescence with fast lifetimes that we termed quasicontinuum photoluminescence (QC-PL). Here, we suggest that a high density of optically active defects leads to QC-PL, where interactions between defects affect the temporal and spectral characteristics of both excitation and emission. We develop a model that predicts the temporal characteristics of QC-PL, based on energy transfer interactions between high densities of defects. Our model does not explain all spectral broadening and redshifts found in QC-PL, since we do not model spectral changes in defects due to proximity to other defects. However, we do provide an example of a well-defined system that exhibits the QC-PL characteristics of a distribution in shortened lifetimes and broadened, redshifted energy levels: an organic chromophore (fluorescein) that has been dried rapidly on a fused silica surface. Recently, we showed that regions of fused silica exposed to up to 1 billion high-fluence laser shots at 351 rm nm at subdamage fluences exhibit significant transmission losses at the surface. Here, we find that these laser-exposed regions also exhibit QC-PL. Increases in the density of induced defects on these laser-exposed surfaces, as measured by the local transmission loss, lead to decreases in the observed lifetime and redshifts in the spectrum of the QC-PL, consistent with our explanation for QC-PL. We have found QC-PL in an increasing variety of situations and materials, and we believe it is a phenomenon commonly found on surfaces and nanostructured materials.

DOI: 10.1103/PhysRevMaterials.1.065201

I. INTRODUCTION

As part of a larger effort to understand light-matter interactions with high-energy and high-power lasers, we have studied the photoluminescence (PL) properties of many materials. We have repeatedly found PL with similar broad excitation and emission properties as well as broad distributions of fast PL lifetimes: in optical materials [1,2], plastics [3,4], and in aggregated silver nanoparticles (discussed here). It initially seemed possible to dismiss this PL as simply a combination of a large variety of transitions on a defective surface. However, the spectral and temporal characteristics of the observed PL do not match any known transitions in the materials. After control studies, these properties could not be dismissed as contamination or as mixtures of known defects in the materials. The one commonality was the presence of high densities of defects, particularly at surfaces. This led to the hypothesis that the high density of defects was responsible for the spectroscopic properties observed.

In the regime where the defect density approaches the atomic density, the electronic structure of the material deviates strongly from descriptions provided by bulk solid state theory or molecular and atomic physics. For sufficient defect densities, significant interactions between defects strongly affect the temporal and spectral characteristics of both excitation and emission of electronic excitations. When multiple photoluminescent species are in close proximity, their spectroscopic properties can change significantly. The lowest energy levels are often shifted to the red, producing broader excitation and emission ranges. Examples include Davydov splitting [5] and excimer formation [6]. Here, we show examples where very high densities of defects or chromophores dramatically change the spectral and temporal properties of the photoluminescent species in highly defective materials and aggregated species. We find that the original spectra are shifted toward the red and smoothed to the point that the final spectra depend primarily on the density of defects present rather than on the identity of the photoluminescent species. Additionally, photoluminescence lifetime distributions are shortened and broadened significantly. In order to describe this PL, we introduced the term quasicontinuum photoluminescence (QC-PL) [2]. QC-PL properties include broad excitation and emission spectra, a broad distribution of PL lifetimes (e.g., from 20 ps to 5 ns), continuous shifts in PL lifetime distributions with respect to emission wavelength, and a propensity to photobleach and photobrighten. The photobleaching and photobrightening effects suggest that systems exhibiting QC-PL are often susceptible to photochemistry.

We have observed QC-PL in several materials with otherwise very distinct properties. We previously reported QC-PL in highly defective materials related to laser-induced damage of optics, including in fused silica, KDP crystals, CaF_2, and redeposited NaCl [1,2,7]. We found photoluminescence with the same spectral and temporal properties in amorphous hydrogenated carbon [3,4]. Others have found the same properties previously [8,9]. Recently, heat-aged polymeric materials were shown to have similar PL [10], where they use the term "density of states PL" to describe what we call QC-PL. Similar PL, including the photobrightening property, has been observed in dry tryptophan particles [11]. We suggest that all of these have similar PL for one reason: a high-density of defects or chromophores interact, causing spread out energy levels and lifetimes.

We previously suggested that the density of defects is inversely related to the observed lifetime of the QC-PL [2,12]. We develop a model for the dependence of the fluorescence

*laurence2@llnl.gov

lifetime characteristics on defect density when a large variety of energy levels are present at high densities. This model is based on the dipole-dipole coupling model due to Förster. This model does not explain the spectral changes to the defect and molecular spectra but does provide a possible explanation for the temporal characteristics observed.

We show several examples demonstrating the dependence of the emission properties and fluorescence lifetime decays on the density of defects or molecular species. We suggest that at sufficient densities and with random distributions, any optically active state will interact with neighbors in such a way as to spread energy levels toward the red and lead to a wide distribution of fast lifetimes. Examples include the standard fluorescent dye fluorescein, defects generated on the surface of silica optics due to long-term exposure to high-laser powers in vacuum, defects developed by laser exposure of a CVD polymer, and aggregated silver nanoparticles.

First, we show the case of the organic fluorophore fluorescein when dried rapidly onto a fused silica surface. The spectra are shifted significantly toward the red, and the lifetimes are shortened to subhundred-picosecond lifetimes. Second, we previously found that exposure of fused silica optics to up to 1 billion high-fluensce subdamage threshold pulses in vacuum leads to transmission losses on those surfaces [13]. Here, we show that these laser-exposed surfaces also exhibit QC-PL, and that the density of induced defects, as measured by the local transmission loss, is inversely related to the observed lifetime of the QC-PL. The spectra are shifted toward the red with increasing transmission loss, providing direct evidence for our previous suggestion that QC-PL properties are related to local densities of defects. The distribution in lifetimes observed is not simply due to a large variety of defect states, but due to a variety of energy transfer interactions between defect states. Third, for amorphous hydrogenated carbon (a-C:H), a polymerlike network typically synthesized by plasma chemical vapor deposition [3,4], we find that the a focused laser beam can affect the density of defects and thus the QC-PL lifetime and spectral characteristics. Finally, we also show that aggregated silver nanoparticles can have similar PL characteristics, albeit with faster lifetimes than observed in other materials. We expect that the characteristics of QC-PL may be found in many highly defective materials, and are of especial significance at surfaces and in nanostructured materials. This is likely a common phenomenon caused by high defect densities, and is an important characteristic that should be accounted for when considering light-matter interactions or performing spectroscopic measurements of any material that may have high densities of photoluminescent species.

II. THEORY

A. Energy transfer and defect densities

The combination of broad excitation and emission, a broad distribution in emission lifetimes, and continuously increasing lifetimes as a function of emission wavelength provides a challenge from a theoretical perspective. For the case of fused silica, the fact that the observed characteristics for QC-PL do not match known defects for silica adds to the puzzle. Here, we do not develop a comprehensive theory to simultaneously explain all of these observations. Rather, we introduce some of the physical effects that we believe are involved, and derive simplified results that can be compared with experiment. Also, based on the model, motivation is provided for additional experiments that test these concepts.

TABLE I. Average spacing of defects as a function of defect density.

Defect density (cm^{-3})	Average defect spacing (nm)
10^{18}	10
10^{19}	4.6
10^{20}	2.2
10^{21}	1
10^{21}	0.46

Our basic hypothesis is that the characteristics of the QC-PL we observe in a variety of materials are primarily due to the high density of defects in the materials, especially on surfaces. Interactions between defects modify the temporal and spectral properties of the defects to such an extent that the defect density is the primary determinant of those properties, rather than the measured properties of the defects at low densities. Table I shows the average defect spacing that corresponds to a series of defect densities. Note that, e.g., fused silica, the concentration of Si-O bonds is 5×10^{22} cm^{-3}, so that defect concentrations above 10^{22} cm^{-3} are not considered. For these high defect densities, average defect spacing is in the nanometer scale.

We hypothesize two primary differences in defect optical properties when defect densities increase to near atomic densities. First, as defect densities increase, long-range, dipole-dipole interactions between defects (often termed Förster resonance energy transfer) would be the first to play a role [14]. These energy transfer processes and possibly electron transfer processes allow electronic excitations to percolate downward through a series of defects (Fig. 1). These interactions can dramatically alter the temporal decay times observed from defects, but, by themselves, will not alter spectral properties. Second, at higher densities, closer range, intrinsically quantum-mechanical interactions between defects will occur. The proximity of defects with each other creates quantum-mechanically interacting complexes of defects, causing the energy levels of the defects to shift, allowing a much wider spectral range of defect levels. This picture results in a high density of spatially localized defect energy levels, each with a unique energy spectrum. This second feature, combined with the random spatial distribution of defects, leads to the broad distribution of PL lifetimes and spectrum observed.

The resulting electronic structure that we envision is as shown in Fig. 1. The energy of the first excited state for defect levels varies rapidly as a function of spatial position. Energy levels of nearly any energy value within the band gap of the host material may be found at some position. The defect levels are very close together so that excitations of a particular defect level may be rapidly transferred to other, lower energy levels via energy transfer processes. We call this situation an energy transfer network since energy transfer interactions cause excitations to be passed to multiple acceptors, likely in succession.

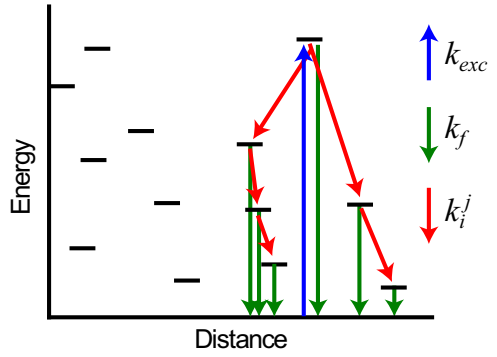

FIG. 1. A large variety of de-excitation pathways are available when there is a high density of defect levels with a variety of energy levels. Upon excitation (k_{exc}), a defect may re-emit a photon, undergo internal conversion without emission of a photon, or undergo intersystem crossing to a triplet state (in the diagram, we ignore intersystem crossing and group the other two processes under k_f). In the presence of other defects, energy transfer via dipole-dipole interactions, higher order interactions, or exchange interactions play a significant or even dominant role (k_i^j). At high enough densities and with a large variety of defect states, successive energy transfers could occur as indicated by red lines.

B. Simulation of energy transfer networks

Beginning with a simple model of an energy transfer network, we use simulations to calculate expected PL lifetime curves as a function of emission energy and to determine if the simulated characteristics match those observed for QC-PL. We simulated PL lifetime curves as a function of energy for the energy transfer network model. A 3D random distribution of defects with specified densities (10^{19} to 10^{21} cm^{-3}) is generated for a given box size (typical 10 μm $\times$ 10 μm $\times$ 1 μm). The defect energy level is randomly chosen between 0 eV and the excitation energy set at 3.5 eV. Each defect is set to have an intrinsic fluorescence lifetime of $k_f = 10$ ns when excited. For each defect, a list is generated of acceptor defects which can accept energy transfer from the current donor defect based on proximity and relative emission and excitation energies. The energy transfer rate is calculated using a dipole-dipole energy transfer process (ignoring polarization effects), assuming $R_0 = 5$ nm for all interactions. The total decay rate for the donor is calculated by adding all of the rates to the interacting acceptors and the intrinsic fluorescence decay rate.

We chose $k_f = 10$ ns to be longer than the lifetimes we observed experimentally (typically up to 5 ns), and we chose $R_0 = 5$ nm to be a typical value for FRET pairs of organic chromophores. R_0 is the distance at which 50% of the donor excitations are transferred to the acceptor if the given donor and acceptor are the only defects present. The R_0 value sets the length scale over which the energy transfer occurs: for a lower R_0, a higher defect density is required for energy transfer to occur. If R_0 is smaller compared to the average defect spacing, then energy transfer would not occur. The spectroscopic properties of donor and acceptor determine R_0, so that any factor such as temperature that affects spectroscopic properties affects R_0. R_0 and k_f can be varied without affecting the basic results obtained, only the numerical values and densities for which these effects are important:

$$k_{\text{Tot}}^j = k_f + \sum_{i=1}^{N_{\text{Acc}}} k_i^j = k_f \left[1 + \sum_{i=1}^{N_{\text{Acc}}} \left(\frac{R_0}{R_{ij}} \right)^6 \right]. \tag{1}$$

A series of limits and cutoffs are used to limit the tabulated interactions to only those that significantly contribute to the decay and to remove pathological (infinite) cases. Interactions between donor and acceptors are ignored if the difference in energy level is greater than 1.0 eV. If the energy transfer rate is less than 0.1 k_f or the quantum efficiency of energy transfer is less than 10^{-3}, those acceptors are excluded. There is also a maximum rate imposed of 10 000 $\times$ kf for every transfer process.

The expected lifetime is calculated by applying an excitation at the laser energy: in our case, 3.5 eV. All defects with energy levels below this level are excited. For each defect, the fluorescence emitted is added to an accumulating lifetime decay array for the energy level of the defect. The decay is calculated according to

$$k_j(t) = \frac{k_f}{k_{\text{Tot}}^j} \exp\left(- k_{\text{Tot}}^j t \right). \tag{2}$$

The factor in front of the exponential is the quantum efficiency. For each acceptor i, the decay of that acceptor is found by calculating the emission as in Eq. (2), but also convolving the acceptor decay with the donor decay:

$$k_i(t) = \left[\frac{k_i^j}{k_f} k_j(t) \right] * \left[\frac{k_f}{k_{\text{Tot}}^i} \exp\left(- k_{\text{Tot}}^i t \right) \right]. \tag{3}$$

The acceptor i can in turn transfer the excitation to its own acceptors. Equation (3) is applied recursively for each acceptor in the chain of possible excitation decay pathways. This leads to the shift to longer lifetimes at lower emission energies, similar to experiments.

C. Energy transfer interactions and fluorescence lifetime

As defect densities in materials increase, interactions between defects are of increasing importance in the optical properties of the material. Sensitized emission of defects in solids via Förster energy transfer from other defects was first described many years ago [14,15]. This mechanism will still be operating at very high defect densities, and may be supplemented by tunneling and electron transfer processes.

The expected fluorescence lifetime decay of a set of donor defects in the presence of a randomly distributed acceptor species has been studied since the 1940s. The model was first worked out in the three-dimensional case by Förster [14]. Additional cases have been worked out subsequently [16–18]. The generalization to fractal dimensions was found in Klafter *et al.* [19]. In general, a stretched exponential model was obtained.

Consider an energy transfer rate between a donor and acceptor of the form

$$\omega(R) = \frac{1}{\tau} \left(\frac{R_0}{R} \right)^s. \tag{4}$$

The rate of emission from a donor species in the presence of an acceptor species with concentration n is [17]

$$k(t) = \exp\left[- V_\Delta n R_0^\Delta \Gamma(1 - \Delta/s)(t/\tau_a)^{\Delta/s}\right]. \quad (5)$$

V_Δ is the volume of unit sphere in Δ dimensions. This expression may also be used for fractal dimensions Δ [19]. By combining many of these parameters, letting $\beta = \Delta/s$ and $\tau_0 = \tau_a[V_\Delta n R_0^\Delta \Gamma(1 - \Delta/s)]^{-\Delta/s}$, a simplified fitting model may be used:

$$P(t) = \frac{A\tau_0}{\Gamma(\beta^{-1})} \exp[-(t/\tau_0)^\beta]. \quad (6)$$

These arguments motivate the use of the stretched exponential fitting function for analyzing fluorescence lifetime decays in this context.

However, for extracting information from fluorescence lifetime decays, caution is warranted in the standard process of fitting the data to the model and in applying specific meaning to the extracted parameters. Often, multiple models fit the data well, and it is necessary to compare the information content of the extracted parameters carefully.

We compare the results from three models: the log-normal distribution, the stretched exponential, and a multiexponential model with fixed lifetime values. We compare results using the resulting distribution of the amplitude densities as a function of lifetime of the resulting fits. The amplitude densities are normalized by the number of photons expected for a given increment in lifetime, not initial amplitude. The signals in fluorescence lifetime measurements are typically in terms of photons, and using the normalization of initial amplitude can overemphasize lifetime components for which there is very limited information. For example, very short lifetimes ($\ll$50 ps) contribute very little signal to the lifetime curve when measured with an instrument response greater than 50 ps, but could have very large fitted initial amplitudes without affecting the result significantly. We will discuss the fitting models in detail and explain how we compare the results of their fits.

D. Multiexponential model

The use of the multiexponential model was discussed in previous publications [1,2] but is reviewed here briefly. In order to accurately extract lifetimes, the finite bin widths, the finite measurement window available between laser pulses, and the measured instrument response must be taken into account. We take T as the time between laser pulses, and as the time resolution of the histogram bins. τ_j is the lifetime of the jth component of the decay model, and IRF_i is the measured instrument response ($i = 0 \ldots n-1$), where $T = n\Delta t$. We define $r_j = T/\tau_j$. A_j is the amplitude of the fitted lifetime curve (equal to the number of photons). The lifetime decay is modeled as in Ref. [20],

$$f_i(\tau) = \left[\sum_j A_j e^{-i\Delta t/\tau_j} \left(\frac{1 - e^{-\Delta t/\tau_j}}{1 - e^{-T/\tau_j}} \right) \right] \times \mathrm{IRF}_i. \quad (7)$$

The symbol $*$ denotes convolution, which is calculated using the fast Fourier transform (FFT). The lifetime components used for our analysis are fixed at 0.04, 0.2, 1.0, and 5.0 ns. We have found these components to be able to fit the lifetime curves we measure well with χ^2 values near 1.0.

E. Log-normal model

The log-normal model is an extension of the multiexponential fit above to a continuous lifetime density with a normal distribution in logarithmic space:

$$P(i\Delta t, \tau_0, \sigma) = A \int_0^\infty \frac{1 - e^{-\Delta t/\tau}}{1 - e^{-T/\tau}} \times \exp[-i\Delta t/\tau - (\ln \tau/\tau_0)^2/2\sigma^2] \frac{d\tau}{\sqrt{2\pi}\tau\sigma}. \quad (8)$$

We convert this expression to logarithmically spaced lifetimes $u = \log_{10} \tau$ to obtain

$$P(i\Delta t, \tau_0, \sigma) = A \int_0^\infty \frac{1 - e^{-\Delta t 10^{-u}}}{1 - e^{-T10^{-u}}} \exp(-i\Delta t 10^{-u}) \times \exp[-(u - \ln \tau_0/\ln 10)^2/2(\sigma/\ln 10)^2] \times \frac{du}{\sqrt{2\pi}\sigma/\ln 10}. \quad (9)$$

The photon density as a function of u for this distribution is simply Gaussian:

$$h(u)du = \exp[-(u - \ln \tau_0/\ln 10)^2/2(\sigma/\ln 10)^2] \times \frac{du}{\sqrt{2\pi}\sigma/\ln 10}. \quad (10)$$

F. Using the stretched exponential and comparing it to other models

The most challenging fitting model for comparisons is the stretched exponential. Due to its mathematical form, it is not easy to compare with functional forms calculated using a distribution of fluorescence lifetimes like the log-normal model described above. In this section, we describe how we use the stretched exponential model to fit lifetime curve data. In Appendix, we develop an asymptotic expansion for the resulting distribution of fluorescence lifetimes for comparison to other models.

For using the stretched exponential model to fit experimental data obtained via time-correlated single-photon counting (TCSPC) [12,20,21], it is necessary for the model to account for the finite bin width of the measurements, and the instrument response. Wraparound of the fluorescence decay due to the high repetition rate of the lasers used for TCSPC must also be taken into account. If the duration of each time bin is Δt, and the time to the next excitation pulse is $N\Delta t$, then integrating Eq. (6), we obtain for the ith bin

$$P_i = \sum_{j=0}^\infty \frac{\tau_0}{1 + \beta^{-1}} \left\{ \Gamma\left[\beta^{-1}, \left(\frac{(jN + i + 1)\Delta t}{\tau_0} \right)^\beta \right] - \Gamma\left[\beta^{-1}, \left(\frac{(jN + i)\Delta t}{\tau_0} \right)^\beta \right] \right\}, \quad (11)$$

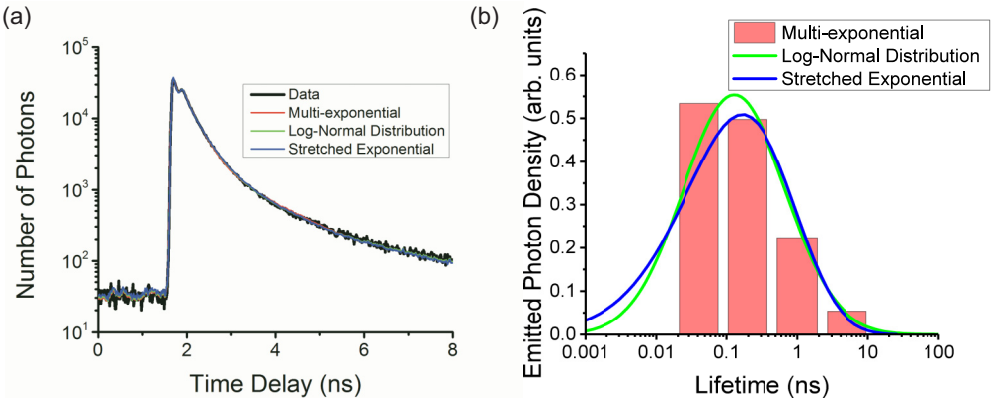

FIG. 2. (a) Fluorescence lifetime decay of 2N silica Vickers indentation on fused silica is fitted to stretched exponential fit, accounting for instrument response and finite bin widths. (b) Normalized residuals plotted for three different fits of the data in part (a). The fits include a four-exponential fit with fixed lifetimes and five parameters, a log-normal model fit with four parameters, and the stretched exponential fit with four parameters.

where $\Gamma(a,x)$ is the incomplete gamma function, and $\Gamma(a)$ is the gamma function. The functional form of Eq. (11) is then convolved with a measured instrument response (IRF_i), and fitted to the data using a maximum likelihood procedure as described in Ref. [21]. One additional fitting parameter in addition to A, τ_0, and β is a temporal shift in the position of the IRF. For practical consideration, the infinite series is truncated.

III. EXPERIMENTAL METHODS

A. PL lifetime imaging and spectroscopy

PL measurements were made on a homebuilt setup described in detail elsewhere [1,2]. Briefly, a 405-nm-wavelength pulsed laser (150 ps) was focused on the sample using a 50×, 0.95 NA objective (Zeiss). PL excited by the laser was collected through the same objective, transmitted through a dichroic mirror (430 DRLP, Omega Optical), and focused onto a 150-μm confocal pinhole. We determine the spectral variation of the fluorescence lifetime properties by placing a monochromator/spectrometer between the detection pinhole and the photon counting APD. The wavelength is scanned during acquisition to obtain the lifetime as a function of wavelength. We use a black-body source (Oriel Model 67030, Newport) to calibrate the spectral profile of detection efficiency. A narrow spectral band of the collected PL was selected using a monochromator/spectrometer (Acton 300i), and focused onto an avalanche photodiode (PDM 50CT, Micro Photon Devices). The PL lifetime was measured by recording the arrival time of each detected photon relative to the laser pulse using a time-to-digital converter (PicoHarp 300, Picoquant).

B. Sample preparation

Dried fluorescein samples were prepared by placing 10 μL of 10 μM fluorescein dissolved in methanol on one of the two fused silica optics prepared as already described. Dried silver nanoparticle samples were prepared by placing 10 μL of solution prepared as described in [22].

The samples with exposures of up to 1 billion high-fluence laser shots were prepared as described previously [13]. Briefly, 2-inch fused silica optics were obtained from Sydor Optics (Rochester, NY) or CVI-Melles Griot (Rochester, NY). Each optic was prepared using an optimized cleaning + etching process as described as AMP2 or AMP3 [7,23]. This process consistently yields high-damage-resistant optics. The sample was mounted in a vacuum chamber under 10^{-6} Torr. The laser shots were conducted with a 351 nm, 3 KHz, 90 ns FWHM laser with average power of 3 W and near Gaussian spatial beam profile (Photonics Industries, Model Number DS-351-4). The beam was focused to the back exit surface of the optic at normal incidence with a FWHM spot size of 1 mm. The 1-mm beam has a pulse intensity of 1.3 MW/cm^2 (pulse fluence 0.12 J/cm^2).

IV. RESULTS AND DISCUSSION

A. Multiple models produce similar lifetime distributions for QC-PL

We first show that the various models developed above allow for quality fits of the fluorescence lifetime curves from QC-PL, and produce similar fluorescence lifetime distributions (Fig. 2). In Fig. 2(a), it can be seen that the quality of fits obtained with the four parameters of the stretched exponential fit, the log-normal model, and the four-exponential fit are comparable (χ^2 of 1.3, 1.3, and 1.2, respectively). All three models provide fits of similar quality over two orders of magnitude in photon arrival time.

We now show that all three models produce similar distributions of amplitudes of fluorescence lifetime. We plot the density of total emitted photons for each lifetime, rather than the initial amplitudes. It is important that the amplitudes of the curves in this case are proportional to the total number of photons detected from each lifetime, not the initial amplitudes of curves from those lifetimes. For example, a given fit from the stretched exponential may predict a large initial amplitude for 1-fs lifetime; however, in terms of the total number of photons produced, it is insignificant. Plotting the distribution as in Fig. 2(b) allows for easy visualization of where significant information was extracted from the lifetime data. By applying the asymptotic expansion of Eq. (21) for the stretched exponential fit, Eq. (11) for the log-normal

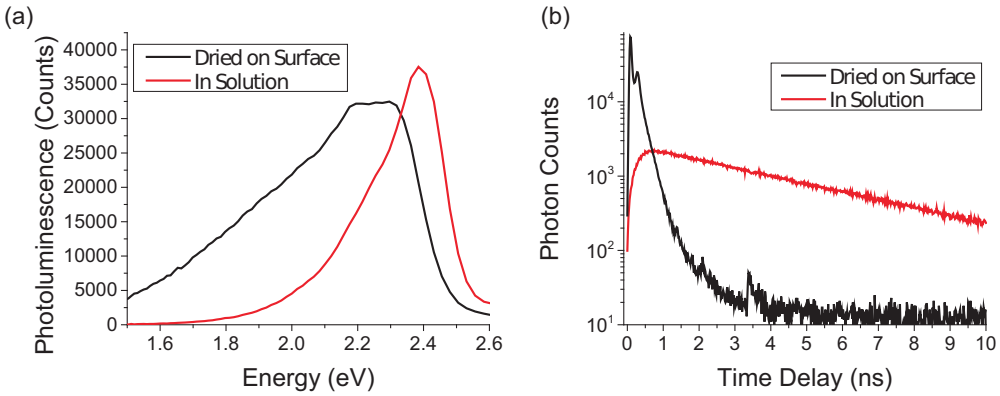

FIG. 3. The organic fluorophore fluorescein is observed to exhibit PL with broad emission and fast lifetimes similar to QC-PL observed in silica when dried rapidly on surfaces, producing a high density of absorbers and emitters at high density. The emission spectrum is redshifted and broadened significantly (a) and the lifetime is shortened dramatically from 3.97 ± 0.05 ns to 0.03 ns or faster (b).

model, and the amplitude for the multiexponential fit, we can directly compare the lifetime distributions fitted for each model. Figure 2(b) shows that there is substantial agreement between these models for lifetime distributions. Regardless of the model chosen for a given QC-PL lifetime curve, it is possible to extract the lifetime distribution using this procedure for comparison. For the remainder of this paper, we use the log-normal model.

B. Density of fluorescent species or defects can affect spectrum and lifetime

If the hypothesis is correct that QC-PL is the result of high densities of defects causing red shifts in energy levels and energy transfer interactions causing broad distributions of fast lifetimes, it should be possible to produce QC-PL with nearly any photoactive system. We have shown elsewhere that amorphous hydrogenated carbon exhibits QC-PL [3,4] as well as other optical materials such as DKDP, SiO_2 and CaF_2 [2].

Here, we use a standard fluorescent dye, fluorescein, which has a well-defined lifetime and spectrum. Fluorescein dissolved in methanol is dried rapidly on a fused silica window, and compared to the fluorescence in solution. The solid formed was yellow, which is likely the zwitterionic form of the solid, which has a measured band gap of 2.3 eV [24]. As shown in Fig. 3, the spectrum is redshifted and widened, and the lifetime is shortened dramatically, consistent with the expectations for an energy transfer network. One difference in this example as compared to the ionic solids is that ordered crystallites likely form, even when dried rapidly. This will reduce the disorder and broadened spectra and lifetimes when compared to defects in solids that occur at random positions. Regardless, it illustrates the redshifting and the shortened lifetime we expect for high densities of photoactive systems.

C. Energy transfer network model produces varying lifetime as function of emission energy

One important property of QC-PL is that the photoluminescence lifetime distribution continuously shifts to slower lifetimes for lower emission energies. We previously hypothesized that this is due to high densities of defects affecting the temporal decays via energy transfer interactions [12]. Here, we show that this photoluminescence lifetime behavior can indeed be explained by energy transfer interactions between defects in close proximity. Figure 4 shows the effects of increasing defect density on the photoluminescence lifetime decays as a function of emission energy. Details of the simulation and calculation may be found in Sec. II B. The defect excitation energies were uniformly distributed up to a 3.5 eV excitation energy for the simulated material. The intrinsic lifetime of each defect, prior to accounting for energy transfer interactions, was set to 10 ns.

As the defect density is increased, the photoluminescence lifetimes decrease dramatically, producing the characteristic lifetime distributions of QC-PL (Fig. 4). At moderately high densities of about 4×10^{19} cm^{-3}, the difference between the lifetime curves for different energies is particularly pronounced. These results help validate the energy transfer network concept, where several successive energy transfer events may take place before final emission of a photon. The center of the lifetime distribution decreases quickly with increasing defect density, as shown in Fig. 4(c), as would be expected for the energy transfer network model.

The spectra of the emitted photons are redshifted for increasing defect densities, as shown in Fig. 4(d). In the simulation, we used a flat emission spectrum as the baseline, which is modified by energy transfer interactions as the defect density increases. For the simulation, much of the emission is for very low energies below 0.5 eV. In the experiments, we do not measure such low-energy photons. Also, we would expect that the quantum efficiency for fluorescence would decrease significantly for lower energy emission. The main result of interest for emission spectrum is the tendency for the energy transfer interactions to cause redshifts in the emission energy spectrum. This does not include redshifts that may come about due to quantum mechanical interactions between defects as the densities increase.

D. Increasing density of defects correlated with decrease in lifetime of QC-PL

By comparing transmission loss imaging, photoluminescence intensity, and photoluminescence lifetime imaging, we provide evidence that the PL lifetime is inversely related to the

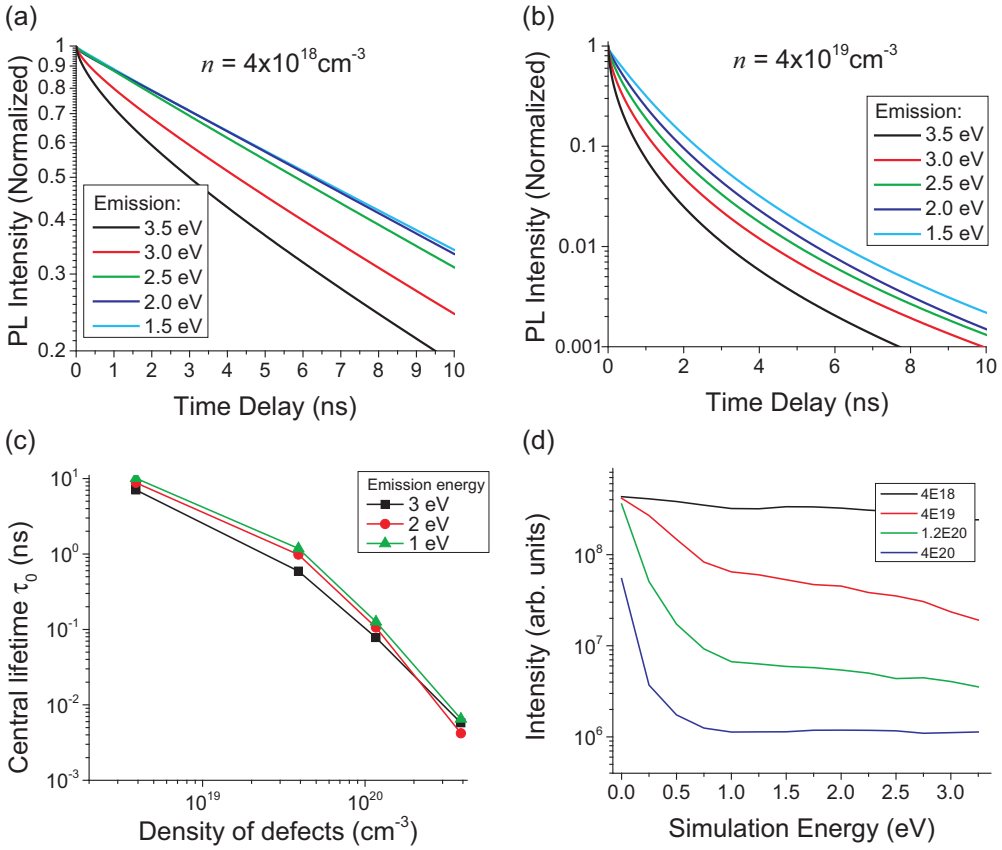

FIG. 4. Fluorescence decay curves as a function of emission energy produced using a simulation based on the energy transfer network concept described in the theory section. The excitation energy is 3.5 eV, and resulting curves are calculated at the noted energies. Curves were calculated for a total of 100000 defects for each given defect concentration. Additional parameters and cutoffs are noted in the text. Total defect concentrations n are noted for each case. (a) $n = 4 \times 10^{18}$ cm^{-3}. (b) $n = 4 \times 10^{19}$ cm^{-3}. (c) Central lifetime τ_0 (ns) as a function of defect concentration n. (d) Calculated emission spectra for the four simulations with different densities of defects. No corrections for the typically decreasing quantum efficiency with lower emission energy were applied.

defect densities producing QC-PL. This evidence is necessary for validating the model for QC-PL that energy transfer interactions indeed play a dominant role in determining the PL lifetime characteristics measured.

1. QC-PL from undamaged, laser-exposed surfaces

Silica surfaces exposed to up to 1 billion high-energy laser pulses show lifetime changes as a function of defect density as measured by transmission loss. We recently found that fused silica surfaces undergo photoactivated chemical reactions when exposed to up to 1 billion high-energy laser pulses in vacuum [13]. These photoinduced reactions lead to a <10 nm surface layer that absorbs a significant fraction of 375-nm light that passes through the surface (up to 4%–5%). High-sensitivity imaging of transmission loss allows for precise quantification of the absorption of this layer as a function of position. We excluded the possibility that the transmission loss was due to scattering by varying the numerical aperture of the collection objectives and by AFM measurements [13]. Such regions also exhibit photoluminescence with the same QC-PL characteristics discussed here and in previous publications [1,2,12]. These sites provide an important test for the hypothesis that increases in defect densities are inversely related to decreases in fluorescence lifetime. The regions with transmission loss are extremely thin (10 nm), without the fractures or roughness associated with other regions containing QC-PL. The transmission loss, and thus the optically active defect density, varies spatially, and can be matched to PL lifetime images for direct comparison.

The effects of defect density as measured by transmission loss on PL lifetime and spectra are shown in Fig. 5. As shown in Fig. 5(a), we exposed different regions of a fused silica sample to varying numbers of high-fluence laser shots in vacuum with a 1-mm Gaussian beam. Increasing the number of shots leads to corresponding increases in transmission loss [5.4×10^6 for S1 to 10^9 for S5, Fig. 5(a)]. There is a corresponding PL signal [Fig. 5(b)] that initially increases, then decreases with increasing shot number. This PL has a broad distribution of lifetimes [Figs. 5(c) and 5(f)], a broad excitation and absorption spectrum [Fig. 5(d)], and a broad emission spectrum [Fig. 5(e)]. These characteristics match those found for QC-PL [2].

The changes in spectra observed in Fig. 5(e) support the hypothesis that for high defect densities the spectra of defects are determined primarily by the density of defects rather than the specific type of defects. In going from region A to region D, the only change is the intensity of the laser beam during

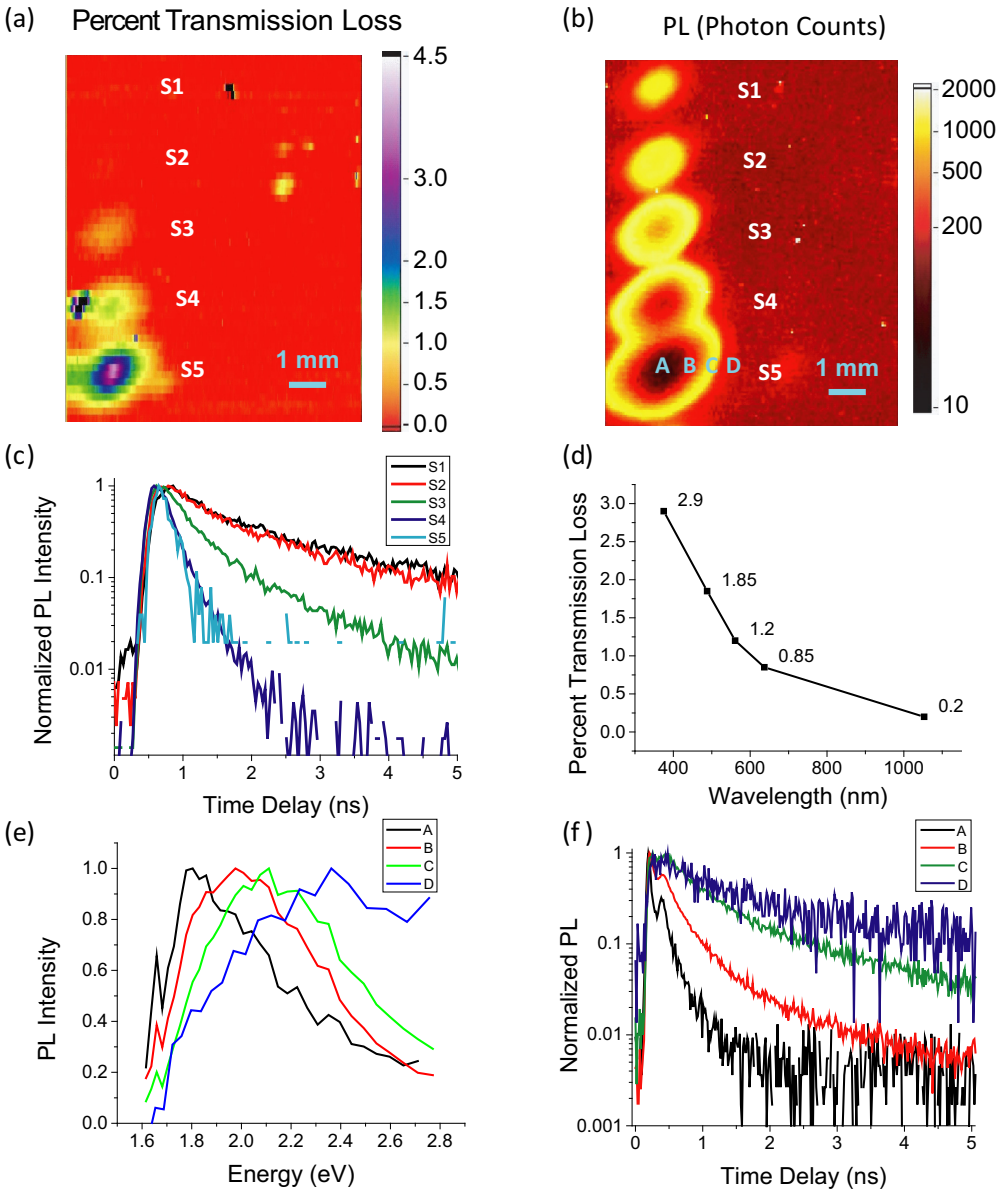

FIG. 5. (a) Transmission images for five laser-exposed sites. S1-S5 are sites exposes to 5.4×10^6, 1.6×10^7, 4.9×10^7, 1.6×10^8, and 1.0×10^9 laser shots. (b) Corresponding images of photoluminescence (PL) measured with 400 nm excitation. Sites A-D are regions of S5 with decreasing density of defects (c) Fluorescence lifetime curves for centers of regions labeled S1-S5 in parts (a) and (b). (d) Percent transmission loss decreases slowly, but consistently as a function of wavelength, indicating a broad absorption spectrum. (e) Within S5, sites A-D exhibit broad emission spectra that are redshifted with increasing defect density. (f) The PL lifetimes also decrease with increasing defect density.

exposure. The peak of the emission spectrum shifts uniformly toward the red with increasing exposure. The alternative explanation of these results is that the emission wavelengths of the types of defects generated by the laser beam depend on the laser beam intensity or total exposure. This alternative explanation seems implausible, given the continuous shifts observed. We conclude that a link between the defect density and the emission spectrum is more likely.

2. *Density dependence of lifetime compared to model*

We now analyze the dependence of the lifetime distribution on the defect density, and compare this dependence to that found in the simulation. In order to make this comparison to simulation, we first make a correlative comparison of the PL characteristics with measured transmission loss in Fig. 6. Since the thin absorbing layer measured in transmission loss imaging is not associated with roughened scattering surfaces, we are able to match the laser intensity to the PL and transmission loss precisely. Focusing on the longest exposure site, S5, we correlate the fitted central lifetime using the log-normal model of the PL intensity [Fig. 6(b)] and the transmission loss [Fig. 6(a)]. Comparing lineouts of total PL intensity with fitted central lifetime [Fig. 6(c)] with lineouts from transmission loss [Fig. 6(d)], it is clear that an increase in PL intensity is initially correlated with a decrease in fitted central lifetime as well as transmission loss. However, the transmission loss and fitted central lifetime are inversely related over all ranges measured

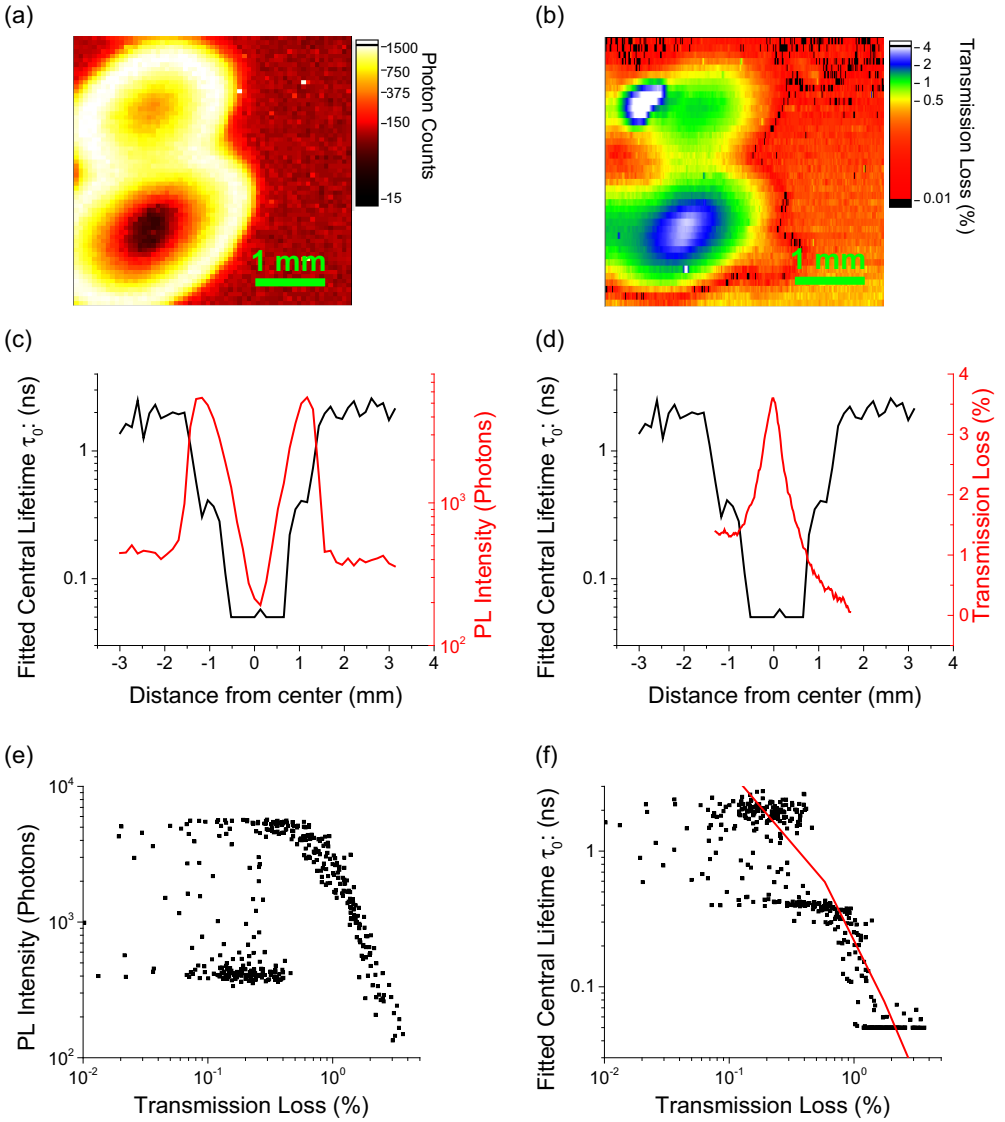

FIG. 6. (a) Photoluminescence image of S1-S5 for uncoated fused silica. The darkest PL corresponds to the regions with the highest transmission losses. (b) Transmission image of exposure sites S5 from Fig. 4 for uncoated fused silica in vacuum. Each pixel was fitted using the Log-Normal distribution model and compared to the transmission loss image. (c) PL Intensity (red) and fitted central lifetime (black) for each pixel of a lineout of S5 from (b). (d) Comparison of same lineout as part (c), but now comparing fitted central lifetime with transmission loss. (e) Scatter plot of PL intensity vs transmission loss shows an increase followed by a decrease. (f) Scatter plot of fitted central lifetime vs transmission loss. The red line is the simulation curve from Fig. 4(c) for 3 eV.

here. Plotting points in a scatter plot directly shows these relationships [Figs. 6(e) and 6(f)]. For the highest transmission losses (above 1%), the PL lifetime is faster than the instrument response of about 50 ps, and the lifetimes default to the minimum fitted lifetime bound of 30 ps. These results support the model that energy transfer processes are involved in QC-PL, and that increases in defect concentration are linked to decreases in observed QC-PL lifetimes.

The experimentally measured dependence of lifetime as a function of defect density matches the simulation dependence as seen in Fig. 6(f). The red line in Fig. 6(f) was replotted from Fig. 4(c), with the density of defects being rescaled to a percent transmission loss (the factor was selected to match the data). The scaled dependence matches the experimental dependence very well, supporting the energy transfer network model for producing the observed lifetime distributions.

In further support that QC-PL is connected with energy transfer processes, we have observed that QC-PL is not strongly polarized, based on polarization measurements through the microscope. The anisotropy is decreased from 0.07 ± 0.01 at 480 nm, 0.10 ± 0.03 at 535 nm, 0.06 ± 0.04 at 580 nm to 0.02 ± 0.05 at 620 nm, and 0.00 ± 0.05 at 665 nm. The relatively large errors are caused by polarization mixing at high numerical aperture and changes in the signal levels during the experiment. In addition, the lifetime decays were not polarization dependent, except in the bluest channel (480 nm), where some difference between the traces can be seen at short times (supplemental information). That the signal is not

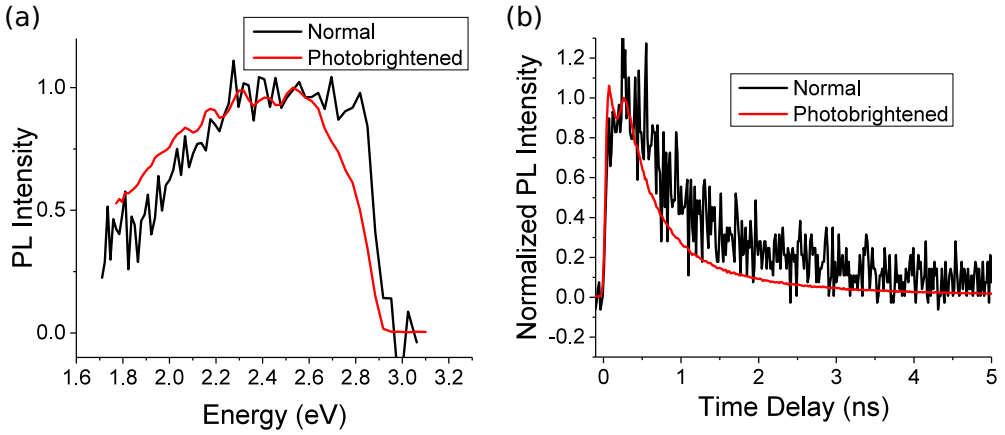

FIG. 7. Effects of higher averaged laser intensity on deposited DVB polymer (150 kW/cm^2 vs 7.6 kW/cm^2, averaged over 40 MHz, 150-ps pulses). Black lines: prior to photobrightening. Red lines: after photobrightening. (a) Spectral peak shifts toward the red. (b) QC-PL lifetimes shift to faster decays, as seen by the sharper peak and faster decay for the red line (photobrightened decay).

strongly polarized is consistent with a depolarizing energy transfer process. This is in agreement with what was observed in "density-of-states" luminescence [10].

E. QC-PL is observed in polymers deposited by chemical vapor deposition

We have shown that the density of defects is related to spectral red shifts and faster lifetime distributions in rapidly dried fluorescein and in long-term exposure of fused silica surfaces to 351-nm laser pulses. We now show an additional case supporting the relationship between defect density and spectrum and lifetime. Divinyl-benzene (DVB) deposited on fused silica was previously shown to have relatively low QC-PL compared to plasma polymers [4]. When exposed to higher laser intensities (150 kW/cm^2 vs 7.6 kW/cm^2), deposited DVB undergoes photobrightening, one of the unusual effects associated with QC-PL as described for surface flaws in fused silica and KDP [2]. Photobrightening increases the defect density, and as shown in Fig. 7, shifts the spectrum toward the red and shortens the lifetime. decreasing the PL lifetime and increases the spectrum (Fig. 7). That the very different materials of silica, KDP, and CVD polymers have similar photoluminescence properties suggests similar physical effects, and supports the conclusions that the QC-PL lifetime and spectrum are related to high defect densities.

F. QC-PL from silver nanoparticles

We also observe QC-PL in silver nanoparticles aggregated on silica surfaces (Fig. 8). The silver nanoparticles were prepared using a method that produces random sizes and aggregates easily [22]. Although we do not expect to find significant PL in metallic systems since there is no band gap, in aggregated metallic nanoparticles there can be a significant density of surface defects or adsorbed molecules. Additionally, the plasmonic effects that give rise to surface effects such as surface-enhanced Raman scattering (SERS) also enhance fluorescence. In this system, we observe the characteristics of QC-PL, including broad emission spectra [Fig. 8(a)], distributions of lifetimes [Fig. 8(b)], and even photobrightening. As shown in Fig. 8, spectra shifted toward the red [comparing samples 1 and 2 in Fig. 8(a)] is associated with faster PL lifetimes [comparing samples 1 and 2 in Fig. 8(b)]. Although other explanations appear to dominate contributions to the SERS continuum background [25], it is

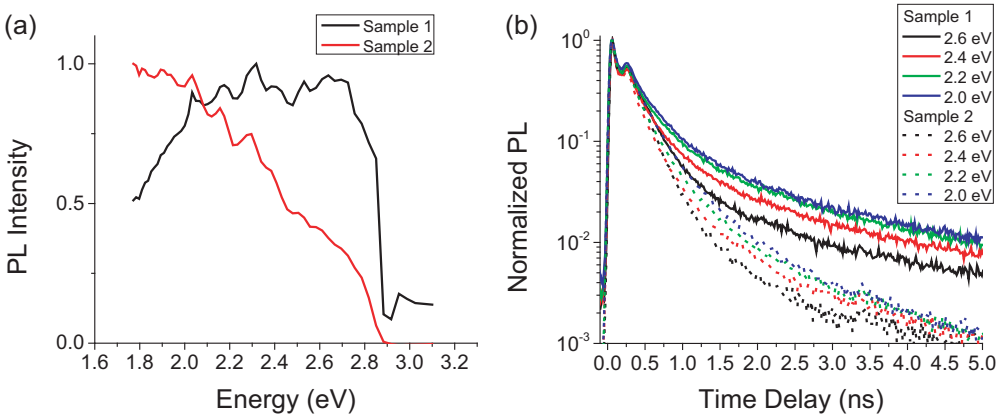

FIG. 8. Silver nanoparticles dried on a fused silica surface exhibit QC-PL characteristics. (a) A broad emission spectrum is observed. (b) A wide distribution of lifetime is also observed, although these lifetimes typically are much faster than those observed in insulating systems.

possible that QC-PL contributes to the background in SERS in certain situations (luminescence has been proposed as a source of background based on time-resolved measurements [26]).

V. CONCLUSION

We have shown how high densities of defects can lead to broad emission profiles and broad distributions of emission lifetimes. Energy transfer interactions are the likely cause of the changing emission lifetimes, whereas the changes in energy levels have a more complicated origin in quantum mechanical interactions. Surfaces of many materials can support such high defect densities, making QC-PL may be a common phenomenon. In fact, this may be the default mode of luminescence for very high defect or chromophore densities. We may find this sort of PL in nanometer-scale systems due to high defect populations and in biological systems.

ACKNOWLEDGMENTS

This work performed under the auspices of the US Department of Energy by Lawrence Livermore National Laboratory under contract DE-AC52-07NA27344 within the LDRD program.

APPENDIX: DISTRIBUTION OF LIFETIMES FOR STRETCHED EXPONENTIAL

Of primary interest in fluorescence lifetime measurements is the distribution of lifetime components. In order to compare any stretched exponential results with other fits, it is necessary to convert the stretched exponential function into the continuous space of lifetime components by performing the inverse Laplace transform. Doing this numerically is problematic since the inverse Laplace transform is ill-posed and sensitive to noise or errors. This cannot be done exactly analytically except in a few select cases, but an asymptotic expansion series can be developed using Watsons lemma [27].

The function $P(t) = N\exp\left[-(t/\tau_0)^\beta\right]$, where $N = [\tau_0\Gamma(1+\beta^{-1})]^{-1}$ can be represented as a distribution of rates k so that

$$P(t) = \int_0^\infty f(k)\exp(-kt)dk = N\exp[-(t/\tau_0)^\beta]. \quad \text{(A1)}$$

This is simply the Laplace transform, which can be inverted using the Mellin inversion formula

$$f(k) = \frac{1}{2\pi i}\int_{\gamma-i\infty}^{\gamma+i\infty} f(k)N\exp(kt)\exp[-(t/\tau_0)^\beta]dt. \quad \text{(A2)}$$

We can calculate this integral using a contour integral in the complex plane. There is a branch cut along the negative real axis. The contour integral contains six individual contours. C_1 is the is contour defined by the Mellin inversion formula in Eq. (A2). C_2 and C_5 are large circular contours in, respectively, quadrants II and III, and in the required limit go to infinity. Contours C_3 and C_5 are along the negative real axis, and C_4 is a small circular contour around the origin that shrinks to 0 radius. Since the integrand has no poles at the origin or within the contour, the total integral is 0,

$$\int_{C_1+\cdots+C_5}\exp(kt)\exp[-(t/\tau_0)^\beta]dt = 0. \quad \text{(A3)}$$

The integral over contour C_1 is, by Eq. (A2), $2\pi i f(k)/N$. The integrals over C_2 and C_5 cancel in the limit to ∞. There is no pole at the origin, so the integral along C_4 goes to 0 in the limit of 0 size. What remains are the integrals on the negative real axis along the branch cut, so that

$$\frac{2\pi i}{N}f(k) + \int_0^\infty \exp(-kt)\exp(-z^*t^\beta)dt - \int_0^\infty \exp(-kt)\exp(-zt^\beta)dt = 0, \quad \text{(A4)}$$

where $z = [\exp(i\pi)/\tau_0]^\beta$. For checking our expansion, $f(k)$ can be calculated in the special case with $\beta = 1/2$, yielding

$$f(k) = \frac{N}{\pi}\int_0^\infty \exp(-kt)\sin(\sqrt{t/\tau_0})dt = \sqrt{\frac{1}{4\pi k^3\tau_0^3}}\exp\left(-\frac{1}{4k\tau_0}\right). \quad \text{(A5)}$$

Using Watson's Lemma in combination with the Taylor expansion

$$\exp(-z^*t^\beta) - \exp(-zt^\beta) = \sum_{p=0}^\infty \frac{t^{\beta p}[(-z^*)^p - (-z)^p]}{p!}, \quad \text{(A6)}$$

the asymptotic expansion of $f(k)$ is

$$f(k)dk = \frac{N}{2\pi i}\sum_{p=0}^\infty \frac{[(-z^*)^p - (-z)^p]}{p!}\frac{\Gamma(\beta p+1)}{k^{\beta p+1}}. \quad \text{(A7)}$$

For comparison to the log-normal and multiexponential models above, we need a density normalized to provide the density of the number of photons expected as a function of the logarithm of lifetime rather than $f(k)$. As a first step to converting this expression, we need to change variables from rate k into lifetime $\tau = 1/k$,

$$P(t) = \int_0^\infty f(k)\exp(-kt)dk = \int_0^\infty f(1/\tau)\exp(-t/\tau)\frac{d\tau}{\tau^2}. \quad \text{(A8)}$$

We change function to $g(\tau)$ so that it is a density of photons emitted in τ space rather than initial amplitude:

$$\int_0^\infty g(1/\tau)\exp(-t/\tau)\frac{d\tau}{\tau} = \int_0^\infty f(1/\tau)\exp(-t/\tau)\frac{d\tau}{\tau^2}, \quad \text{(A9)}$$

so that $g(\tau) = f(1/\tau)/\tau$. In a similar way, we then convert $g(\tau)$ to logarithmically spaced lifetimes $u = \log_{10}\tau$ to obtain $h(u)du$:

$$h(u)du = \frac{N}{2\pi i}\sum_{p=0}^{\infty}\frac{[(-z^*)^p - (-z)^p]}{p!}\Gamma(\beta p + 1)10^{u(\beta p+1)}\ln(10)du. \tag{A10}$$

This expression was used to calculate the distribution shown in Fig. 2(b).

[1] T. A. Laurence, J. D. Bude, N. Shen, T. Feldman, P. E. Miller, W. A. Steele, and T. Suratwala, Appl. Phys. Lett. **94**, 151114 (2009).

[2] T. A. Laurence, J. D. Bude, N. Shen, W. A. Steele, and S. Ly, J. Appl. Phys. **115**, 083501 (2014).

[3] S. Baxamusa, T. Laurence, M. Worthington, and P. Ehrmann, Polym. Degrad. Stab. **122**, 133 (2015).

[4] S. H. Baxamusa, A. Suresh, P. Ehrmann, T. Laurence, J. Hanania, J. Hayes, S. Harley, and D. D. Burkey, Chem. Vap. Deposition **21**, 267 (2015).

[5] T. N. Misra, Rev. Pure Appl. Chem. **15**, 39 (1965).

[6] F. Hirayama, J. Chem. Phys. **42**, 3163 (1965).

[7] J. Bude, P. Miller, S. Baxamusa, N. Shen, T. Laurence, W. Steele, T. Suratwala, L. Wong, W. Carr, D. Cross, and M. Monticelli, Opt. Express **22**, 5839 (2014).

[8] W. Lormes, M. Hundhausen, and L. Ley, J. Non-Cryst. Solids **227-230**, Part 1, 570 (1998).

[9] M. N. Berberan-Santos, A. Fedorov, J. P. Conde, C. Godet, T. Heitz, and J. E. Boure, Chem. Phys. Lett. **319**, 113 (2000).

[10] R. Steffen, G. Wallner, J. Rekstad, and B. Rder, Polym. Degrad. Stab. **134**, 49 (2016).

[11] C. W. Lai, M. Schwab, S. C. Hill, J. Santarpia, and Y.-L. Pan, Opt. Express **24**, 11654 (2016).

[12] T. A. Laurence, J. D. Bude, and N. Shen, MRS Online Proceedings Library **1365**, mrss11-1365-tt08-04 (2011).

[13] S. Ly, T. A. Laurence, N. Shen, B. Hollingsworth, M. Norton, and J. D. Bude, Opt. Express **23**, 4074 (2015).

[14] T. Förster, Z. Naturforsch., A **4**, 321 (1949).

[15] D. L. Dexter, J. Chem. Phys. **21**, 836 (1953).

[16] A. Blumen, J. Chem. Phys. **72**, 2632 (1980).

[17] A. Blumen, Nuovo Cimento Soc. Ital. Fis., B **63**, 50 (1981).

[18] M. Inokuti and F. Hirayama, J. Chem. Phys. **43**, 1978 (1965).

[19] J. Klafter and A. Blumen, J. Chem. Phys. **80**, 875 (1984).

[20] C. Zander, M. Sauer, K. H. Drexhage, D.-S. Ko, A. Schulz, J. Wolfrum, L. Brand, C. Eggeling, and C. A. M. Seidel, Appl. Phys. B **63**, 517 (1996).

[21] T. A. Laurence and B. A. Chromy, Nat. Meth. **7**, 338 (2010).

[22] P. C. Lee and D. Meisel, J. Phys. Chem. **86**, 3391 (1982).

[23] T. I. Suratwala, P. E. Miller, J. D. Bude, W. A. Steele, N. Shen, M. V. Monticelli, M. D. Feit, T. A. Laurence, M. A. Norton, C. W. Carr, and L. L. Wong, J. Am. Ceram. Soc. **94**, 416 (2011).

[24] M. Arhangelskis, M. D. Eddleston, D. G. Reid, G. M. Day, D.-K. Buar, A. J. Morris, and W. Jones, Chem. Eur. J. **22**, 10065 (2016).

[25] S. M. Barnett, N. Harris, and J. J. Baumberg, Phys. Chem. Chem. Phys. **16**, 6544 (2014).

[26] J. P. Heritage, J. G. Bergman, A. Pinczuk, and J. M. Worlock, Chem. Phys. Lett. **67**, 229 (1979).

[27] E. T. Copson, *Asymptotic Expansions* (Cambridge University Press, Cambridge, 1965).